XLIII CILAMCE
21–25, November, 2022
FOZ DO IGUAÇU – PR – BRAZIL

# COMPARATIVE ANALYSIS BETWEEN TURBULENCE MODELS FOR THE RECTANGULAR 2:1 CROSS SECTION

Juliema Fronczak[1],Alexandre Miguel Silva Araújo[1], Gabriel Antonio Mendes das Flores[1], Alexandre A. Cury[3], Patricia Habib Hallak[3]

[1]*Postgraduate Program in Civil Engineering, Federal University of Juiz de Fora*
*José Lourenço Kelmer Street, São Pedro, 36036-900, Minas Gerais/Juiz de Fora, Brazil*
*juliema.fronczak@engenharia.ufjf.br, araujo.alexandre@engenharia.ufjf.br,*
*gabriel.flores@engenharia.ufjf.br*
[3]*Dept. of Computational and Applied Mechanics, Federal University of Juiz de Fora*
*José Lourenço Kelmer Street, São Pedro, 36036-900, Minas Gerais/Juiz de Fora, Brazil*
*alexandre.cury@ufjf.edu.br, patricia.hallak@ufjf.edu.br*

**Abstract.** Flow around rectangular structures is a classic topic in computer simulation due to its incidence and characteristic similar to structures in engineering such as tall buildings, bridge decks, water treatment plants, etc. Therefore, this work discusses the results of two-dimensional computational fluid dynamics simulations of turbulent flow, performed for a rectangular cylinder with Re=$10^5$. The Navier-Stokes equations were solved with Reynolds mean turbulence models, specifically, k-$\omega$ $SST$, k-$\omega$ $SST$ $LM$, k-$\varepsilon$. The simulations performed are used as a parameter for a comparative analysis of the performance of these turbulence models. The objective of the research is to carry out a discussion about the presented turbulence models, making a correlation with the coefficients of drag, lift, Strouhal number and the pressure coefficient around the studied section. The analysis showed that for the case studies considered, the k $\omega$ $SST$ and k $\omega$ $SST$ $LM$ models were able to provide results closer to the literature when compared to the others. All developments were performed with non-commercial OpenFoam code.

**Keywords:** CFD, OpenFoam, Rectangular Section, Aeroelasticity

## 1 Introduction

Understanding how turbulent flow behaves around a rectangular cylinder is a challenge, due to its random nature, turbulent flow is defined by probabilistic laws that allow, through local averages, to estimate its behavior. With the increase in computational resources, allowing high-resolution solutions, some methods have emerged that make it possible to predict the turbulent flow. As several turbulence models have been developed in the last decades, evaluating the generality of the behavior in some aerodynamic coefficients is essential. Thus, the performance of three turbulence models was assessed, for a turbulent, incompressible flow with a Reynolds number of $10^5$. The models studied are linear and include most of the computational fluid dynamics (CFD) approaches, consequently covering the method used in this research, the Reynolds Means of the Navier-Stokes Equation (RANS).

The turbulence models with two equations are the $k$-$\varepsilon$ and the $k$-$\omega$ $SST$. The model $k$-$\omega$ $SST$ $LM$ has four equations. The research analyzed these models in turbulent flow in contact with a 2:1 rectangular section (B/D). The dimensionless parameters chosen for this analysis were the average of the Drag Coefficients ($C_D$) and Lift ($C_L$), RMS of the Lift Coefficient ($C'_L$), Strohaul ($St$) and the average and RMS of the Pressure Coefficient ($C_p$ and $C'_p$), all of them compared with experimental and numerical data found in the literature.

## 2 Theoretical basis

### 2.1 Governing equations in fluid dynamics

A flow characterized by a constant and incompressible viscosity can be described by the physical-mathematical model of the Navier-Stokes equations. The equations 1 and 2 represent the balance of the entities of momentum

and conservation of mass respectively,

$$\nabla.\vec{u} = 0, \tag{1}$$

$$\rho\frac{\partial\vec{u}}{\partial t} + \rho\nabla.\vec{u}\vec{u} = -\nabla p + \nabla.(\bar{\bar{\tau}}) + \rho\vec{g} + \vec{F} \tag{2}$$

the term $\rho$ represents the flow density; $p$, the pressure; $\mu$, is the dynamic viscosity; $\vec{u}$ the velocity field; $\widetilde{\bar{\tau}} = \mu\left[\left(\nabla\vec{v} + \nabla\vec{v}^T\right)\right]$ the tension tensor ; $\rho\vec{g}$ and $\vec{F}$ are respectively the gravitational forces and external forces.

### 2.2 Aerodynamic forces coefficients

The drag coefficient $C_D$ and lift coefficient $C_L$ per unit length were evaluated, in addition to the average pressure coefficient $C_p$,

$$C_D = \frac{F_D}{\frac{1}{2}\rho U^2 B}; \quad C_L = \frac{F_L}{\frac{1}{2}\rho U^2 B}; \quad C_p = \frac{p}{\frac{1}{2}\rho U^2} \tag{3}$$

where U is the reference velocity field, $F_D$ and $F_L$ are the average drag and lift forces, $\rho$ is the air density, B is the characteristic dimension of the section, which, for the present study, is considered as the projected width of the rectangular section normal to the flow direction. Also, the Strouhal number $St$ was calculated as:

$$St = \frac{f_s B}{U} \tag{4}$$

where $f_s$ is the frequency of vortex shedding.

### 2.3 Turbulence properties

For the RANS method, the turbulence models $k$-$\varepsilon$, $k$-$\omega$ $SST$ and $k$-$\omega$ $SST$ $LM$ were applied as discussed in the section 1, all these models are linear and based on the Boussinesq hypothesis, where there is a relationship between the turbulent stresses and the average strain rate tensor through the isotropic viscosity of the vortices. Boussinesq's hypothesis for the constitutive relationship is defined by:

$$\tau_{ij} = 2\mu_t\left(S_{ij} - \frac{1}{3}\frac{\partial u_k}{\partial x_k}\delta_{ij}\right) - \frac{2}{3}\rho k\delta_{ij} \tag{5}$$

where $\mu_t$ is the turbulent viscosity associated locally with the flow, $S_{ij}$ represents the average strain rate tensor of the fluid, k is the turbulent kinetic energy.

The $k$-$\varepsilon$ turbulence model according to [1] has an excellent prediction in hydrodynamics and thermal consequences of acceleration. This model solves two entities, the turbulent kinetic energy dissipation rate term $\varepsilon$ represented by the transport equation 7 and the kinetic energy term defined by 6

$$\underbrace{\frac{\partial(\rho k)}{\partial t}}_{Time} + \underbrace{\nabla.(\rho\mathbf{u}k)}_{Convection} = \underbrace{\nabla.\left[\left(\mu + \frac{\mu_t}{\sigma k}\right)\nabla k\right]}_{Diffusion} + \underbrace{P_k + P_b + S_k}_{Sources+Sinks} \tag{6}$$

$$\underbrace{\frac{\partial\rho\varepsilon}{\partial t}}_{Time} + \underbrace{\nabla.(\rho\mathbf{u}\varepsilon)}_{Convection} = \underbrace{\nabla.\left[\left(\mu + \frac{\mu_t}{\sigma\varepsilon}\right)\nabla\varepsilon\right]}_{Diffusion} + \underbrace{C_1\frac{\varepsilon}{k}(P_k + C_3P_D) - C_2\rho\frac{\varepsilon^2}{k} + S_\varepsilon}_{Sources+Sinks} \tag{7}$$

the coefficients $C_1$, $C_2$ and $C_3$ vary according to the model used and in this work the reference values of [2] were used. The term $P_k$ is the production due to mean shear rate, $P_b$ is the production due to fluctuations, $S_k$ source definition. The $k$-$\omega$ $SST$ turbulence model was implemented according to [3]. The model is given by two equations, the equation 6 and the equation 8 that convey the specific rate and dissipation of turbulence defined by the hypothesis of [4]:

$$\frac{\partial\rho\omega}{\partial t} + \nabla(\rho U\omega) = \nabla\left[\left(\mu + \frac{\mu_t}{\sigma_k}\right)\nabla_\omega\right] + \frac{\gamma}{\nu_t}P_k - \beta\rho\omega^2 + \frac{2\rho\sigma\omega^2}{\omega}\nabla_k : \nabla_\omega \tag{8}$$

where $\gamma$ and $\beta$ are auxiliary constants.

Langtry and Menter [5] developed a transition model based on correlations. The model is based on four transport equations, the equations 6 and 8, presented earlier, plus one for intermittence $\gamma$ and another for a transition

start criterion in terms of the number of Reynolds moment-thickness $\hat{R}e_{\theta t}$. This model, $k$-$\omega$ $SST$ $LM$, is also known as the $\gamma$-$\hat{R}e_{\theta t}$-$SST$ model, because it is based on the equations of $\gamma$ and $\hat{R}e_{\theta t}$, in addition to the equations $k$ and $\omega$.

$$\frac{\partial(\rho\gamma)}{\partial t} + \frac{\partial \rho U \gamma}{\partial x} = P_\gamma - E_\gamma + \frac{\partial}{\partial x}\left[\left(\mu + \frac{\mu_t}{\sigma_f}\right)\frac{\partial \gamma}{\partial x}\right] \tag{9}$$

$$\frac{\partial(\rho\hat{R}e_{\theta t})}{\partial t} + \frac{\partial \rho u \hat{R}e_{\theta t}}{\partial x} = P_{\theta t} + \frac{\partial}{\partial x}\left[\sigma_{\theta t}\left(\mu + \mu_t\right)\frac{\partial \hat{R}e_{\theta t}}{\partial x}\right] \tag{10}$$

the source terms of the 9 equation are $P_\gamma$ and $E_\gamma$, the term $P_{\theta t}$ being the very definition of the source term of the 10 equation.

## 3 Simulation results and discussion

The results of the simulations are presented in this section, for two-dimensional flow, and the Reynolds number is equal to $10^5$.

A series of results were obtained through this simulation, such as the time-averaged global quantities, the Strouhal number (St), the mean pressure around the structure ($C_p$) and the fluctuation ($C'_p$), the mean and the RMS values of lift ($C_L$ and $C'_L$) and drag force. The simulations were performed with the turbulence models presented in Section 2.3 and the results were compared to the reference values available in the literature.

### 3.1 Boundary conditions

In this study, the dimensions of the problem domain for the 2:1 rectangular section are shown in Figure 1. The problem is described in a Cartesian system (x,y,z) in which the flow is perpendicular to the x-axis as can be seen in the figure 1. The 2:1 cylinder (B/D) is exposed to an incompressible flow $U_\infty$ and a constant viscosity.

The boundary conditions for the studied geometry were defined in OpenFoam, the properties are shown below:

- In the $inlet$ the uniform flow is specified in the input by $U_\infty$, which has Reynolds defined by the Equation 11, where $U$ is the fluid flow, $\rho$ is the density, $B$ the characteristic length and $\mu$ is defined by the dynamic viscosity.

$$Re = \frac{\rho U B}{\mu} \tag{11}$$

- The $outlet$ has 60 units of length from the center of the rectangular geometry and has values for the velocity gradient and the relative pressure, equal to zero.
- For the limits $Top$ and $Bottom$ defined in Figure 1, there is a movement with a speed of 1 m/s in the x-direction, so it requires a fixedValue condition with uniform value (1 0 0), both are given a zeroGradient boundary condition for p, which means that the normal pressure gradient is zero.

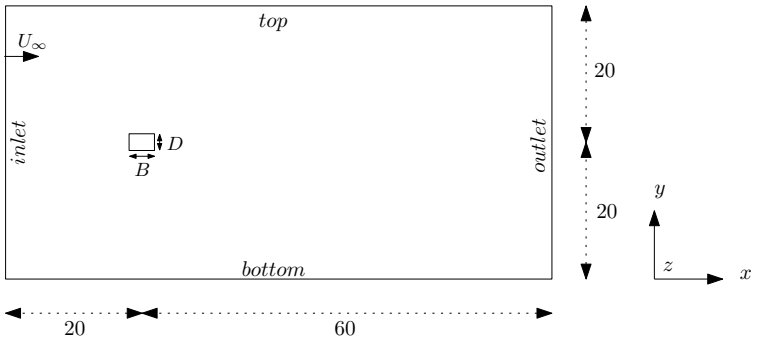


Figure 1. Fluid domain and boundary conditions

### 3.2 Mesh independence test at static cases

A mesh refinement study was performed. Table 1 presents the characteristics of the meshes. The meshes were submitted to the convergence test, that is, for each turbulence model studied, a comparison with the reference values was performed.

Table 1. Mesh independence test carried out for flow past a rectangular cylinder at static cases

| Meshes | Number of nodes / Elements | Aspect ratio | Skewness |
|---|---|---|---|
| Mesh 1 | 40192 / 119532 | 2.16 | 0.49 |
| Mesh 2 | 61876 / 184324 | 2.32 | 0.47 |
| Mesh 3 | 113493 / 338738 | 2.30 | 0.47 |

For the mesh convergence analysis, dimensionless parameters were used that represent important characteristics for the study of the flow behavior through the session, the results are presented in Table 2. The analysis was performed for all turbulence models studied and the results obtained were similar to those in the literature. It is observed, with the analysis of the chosen parameters, $C_D$, $C'_L$, and $S_t$, it is possible to analyze that there is no significant difference in their values for each of the meshes, however, the greater the number of elements higher the computational cost in obtaining the results. Therefore, for comparisons and subsequent simulations, mesh 2 was used. Figure 2 shows details of the mesh around the surface of the rectangle.

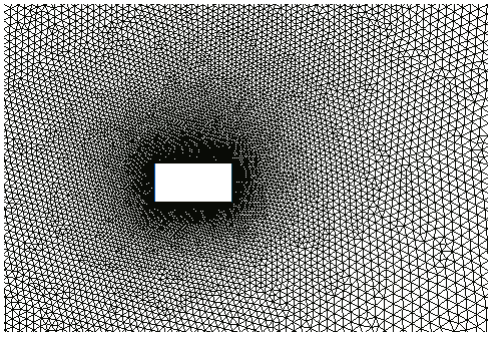

Figure 2. Unstructured mesh around rectangular section

Table 2. Mesh independence test carried out for flow past a rectangular cylinder at static cases

| Meshes | $k$-$\varepsilon$ | | | $k$-$\omega$ $SST$ | | | $k$-$\omega$ $SST$ $LM$ | | |
|---|---|---|---|---|---|---|---|---|---|
| | $C_D$ | $C'_L$ | $St$ | $C_D$ | $C'_L$ | $St$ | $C_D$ | $C'_L$ | $St$ |
| Mesh 1 | 0.60 | 0.0038 | 0.048 | 0.71 | 0.63 | 0.061 | 0.68 | 0.55 | 0.073 |
| Mesh 2 | 0.61 | 0.0033 | 0.048 | 0.70 | 0.60 | 0.061 | 0.68 | 0.43 | 0.073 |
| Mesh 3 | 0.62 | 0.0053 | 0.048 | 0.71 | 0.67 | 0.061 | 0.70 | 0.32 | 0.073 |
| Literature review | | | | | | | | | |
| | $C_D$ | $C'_L$ | $St$ | | | | | | |
| Yu and Kareem(1998) [6] | 0.84 | 0.6115 | 0.080 | | | | | | |
| Keerthana and Harikrishna (2017) [7] | 0.69 | 0.65 | 0.084 | | | | | | |

### 3.3 Angle of attack

In this section, the dimensionless aerodynamic coefficients, $C_D$ and $C_L$ for moderate angles of attack concerning the flow are presented, comparing the results obtained by the turbulence models presented in Section 2.3.

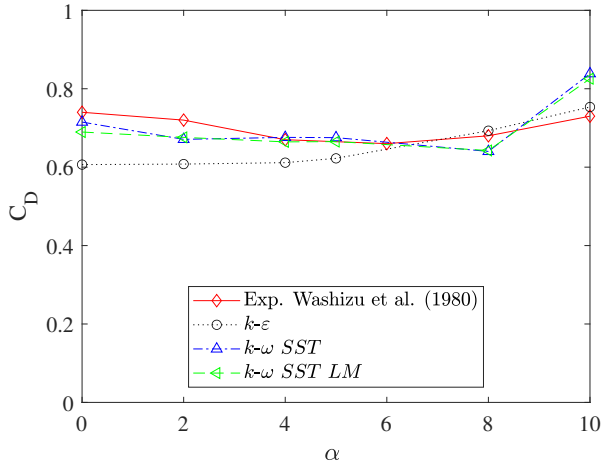


Figure 3. Variation of the $C_D$ with the attack angle

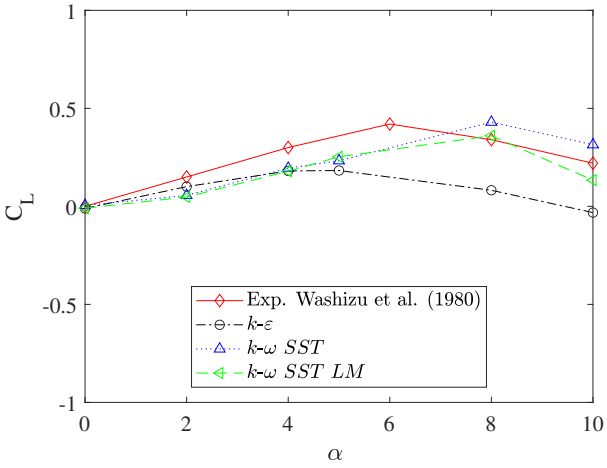


Figure 4. Variation of the $C_L$ with the attack angle

Observing the Figures 3 and 4 referring to the variation of the aerodynamic dimensionless coefficients at the angle of attack, it is possible to observe that there was no great variation in the values obtained from the different turbulence models studied. Making a comparison with the reference values of Washizu et al. [8], for $C_D$, as the angle of attack increases there is a small approximation of the turbulence model $k$-$\varepsilon$ to the reference value. When we make this comparison with $C_L$, we observe a departure from $k$-$\varepsilon$ and, in general, the turbulence models $k$-$\omega$ $SST$ and $k$-$\omega$ $SST$ $LM$ behaved better.

Table 3. Computing time

| Angle | $k$-$\varepsilon$ | $k$-$\omega$ $SST$ | $k$-$\omega$ $SST$ $LM$ |
|---|---|---|---|
| 2° | 2h19min | 4h45min | 2h12min |
| 5° | 4h41min | 5h25min | 1h57min |
| 10° | 3h50min | 2h45min | 2h20min |

The accuracy of the models was also analyzed due to the computational cost, another important aspect regarding the performance of the models. All RANS simulations for the models presented in Section 2.3 were conducted on a computer with an Intel(R) Core(TM) i5 CPU, with 8 GB of RAM memory and system Windows 10 Pro 64-bit operating system. According to [9], four fundamental factors usually influence the processing time of simulations: mesh density; discretization scheme; degree of linearity of the model, and the number of PDEs that the model contains. In this study, the mesh density and the discretization scheme were fixed, that is, the difference in simulation time presented in the 3 table is entirely attributed to the turbulence model itself.

The model with two equations, o $k$-$\varepsilon$, was the one that presented better results when compared to the model $k$-$\omega$ $SST$. However, comparing the three turbulence models, the model $k$-$\omega$ $SST$ $LM$ had the lowest computational cost.

### 3.4 Mean pressure

To investigate the effect of the distribution of the mean pressure coefficient around a rectangular cylinder, a comparison was made with the numerical data of Shimada and Ishihara [10] and of Yu and Kareem [6]. Figure 5 shows the distribution of the mean pressure force ($C_p$) and Figure 6 presents the study of fluctuating pressures ($C_p^{'}$), both along with the upper side of the studied section, defined by the dimension 'B' in Figure 1.

The average distribution of the pressure coefficient in the studied section shows an excellent agreement for the zero incidence angle with the numerical results of the literature. Comparing with the results extracted in the simulations of the $k$-$\varepsilon$ turbulence model, it is possible to observe a discrepancy in the behavior when compared to the reference values, since the distribution of the results of Yu and Kareem [6] and Shimada and Ishihara [10] is almost uniform with a small variation in the final part in the rectangular section, that is, the turbulence model $k-$ did not show good performance when compared to the models $k-\omega$ $SST$ and $k-\omega$ $SST$ $LM$. In Figure 6, the RMS pressure fluctuations on the upper face of the rectangular cylinder are also compared with the different

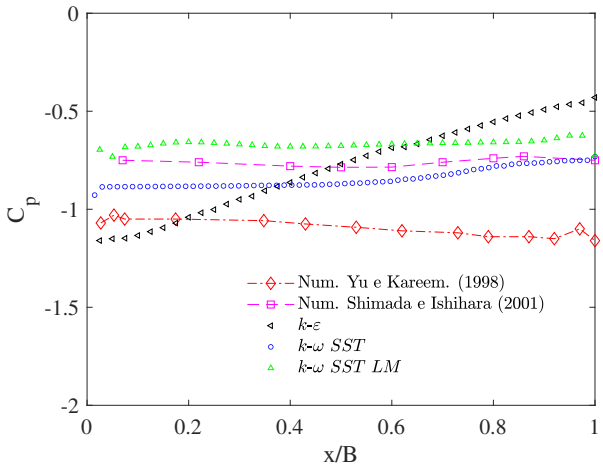


Figure 5. Mean of the pressure coefficients along the of the cross-section of the rectangular 2:1 cylinder

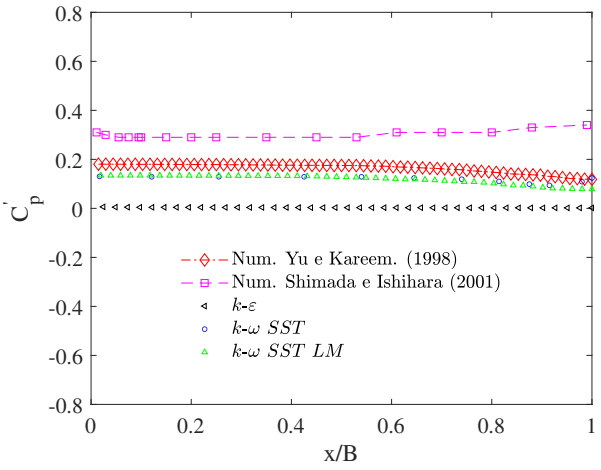


Figure 6. Comparison of RMS of pressure fluctuations on the side face of rectangular prisms with different turbulence model

turbulence models. In this case, the models $k$-$\omega$ $SST$ and $k$-$\omega$ $SST$ $LM$ had results that almost coincided with the reference value of Yu and Kareem [6], while the turbulence model $k$-$\varepsilon$ obtained a small discrepancy of the two references.

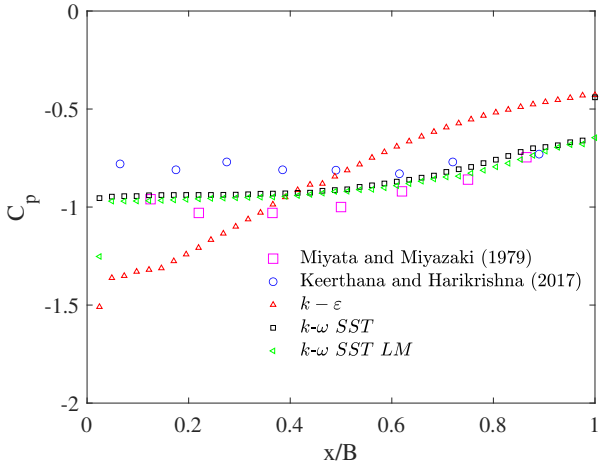


Figure 7. Mean of the pressure coefficients along the of the cross-section of the rectangular 2:1 cylinder at 4º angle of attack

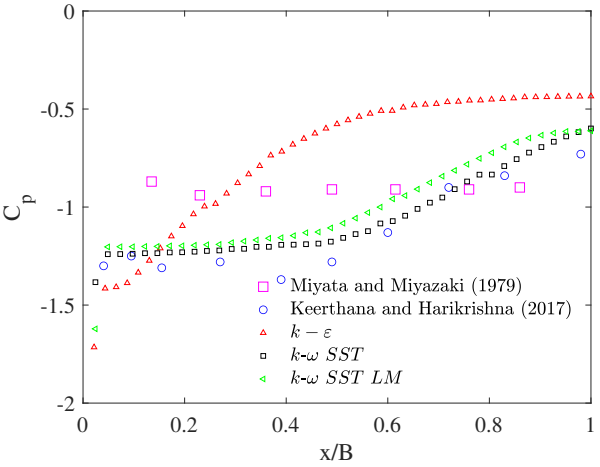


Figure 8. Mean of the pressure coefficients along the of the cross-section of the rectangular 2:1 cylinder at 8º angle of attack

Figures 7 and 8 show the values of the average pressure coefficient when the structure presents angles of attack equal to 4º and 8º respectively, both counterclockwise. It is possible to verify that as the incidence angle increases, there is a decrease in the average pressure coefficient at the beginning of the structure. The turbulence models $k$-$\omega$ $SST$ and $k$-$\omega$ $SST$ $LM$ had similar results, both within the range of reference values, whereas the turbulence model $k$ -$\varepsilon$ exhibited an outlier behavior.

## 4 Conclusions

A numerical study of the flow around a rectangular cylinder with a Reynolds number $10^5$ was performed using the RANS simulation method. Based on a mesh refinement study, a mesh with good convergence was selected for this study. The variations of the flow parameters caused by the different turbulence models are clearly illustrated both in the graphs with average forces over time and in the pressure distribution results. The numerical results of the general lift and drag forces and the Strouhal numbers are in good agreement with the numerical and

experimental values available. The aerodynamic coefficients were calculated from stationary analysis at angles of attack in the range of 0 to 10 degrees, for the three turbulence models, $k$-$\varepsilon$, $k$-$\omega$ $SST$ and $k$-$\omega$ $SST$ $LM$. The comparative analysis between the results of the simulations with three different models of turbulence and the results of the literature, experimental and numerical, allow to highlight some important points. In the analysis of the pressure coefficient around the section studied, it is possible to observe that as the angle of incidence increased, the turbulence model $k$-$\varepsilon$ moved even further away from the reference values, whereas the models $k$-$\omega$ $SST$ and $k$-$\omega$ $SST$ $LM$, in general, both methods performed very well for this simplified section. Considering the computational cost plus the performance of the turbulence model to the aerodynamic coefficients, the model $k$-$\omega$ $SST$ $LM$ had the best performance, with excellent results when compared to the reference values and a low computational cost.

## References

[1] W. P. JONES and B. E. LAUNDER. the Prediction of Laminarization With a Two-Equation Model of Turbulence. *a.I.a.a. Selected Reprint Series*, vol. 14 : TURBULENCE TRANSPORT MODELING, n. (FEBRUARY, 1973), pp. 119–132, 1973.

[2] B. E. Launder and D. B. Spalding. The numerical computation of turbulent flows. *Computer Methods in Applied Mechanics and Engineering*, vol. 3, n. 2, pp. 269–289, 1974.

[3] F. R. Menter. Two-equation eddy-viscosity turbulence models for engineering applications. *AIAA Journal*, vol. 32, n. 8, pp. 1598–1605, 1994.

[4] P. BRADSHAW. Possible origin of Prandt's mixing-length theory. *Nature*, vol. 249, n. 5453, 1974.

[5] R. B. Langtry and F. R. Menter. Correlation-based transition modeling for unstructured parallelized computational fluid dynamics codes. *AIAA Journal*, vol. 47, n. 12, pp. 2894–2906, 2009.

[6] D. Yu and A. Kareem. Parametric study of flow around rectangular prisms using LES. *Journal of Wind Engineering and Industrial Aerodynamics*, vol. 77-78, pp. 653–662, 1998.

[7] M. Keerthana and P. Harikrishna. Wind tunnel investigations on aerodynamics of a 2:1 rectangular section for various angles of wind incidence. *Wind and Structures, An International Journal*, vol. 25, n. 3, pp. 301–328, 2017.

[8] K. Washizu, A. Ohya, Y. Otsuki, and K. Fujii. Aeroelastic instability of rectangular cylinders in a torsional mode due to a transverse wind. *Journal of Sound and Vibration*, vol. 72, n. 4, pp. 507–521, 1980.

[9] Z. Zhang, W. Zhang, Z. J. Zhai, Q. Y. Chen, Z. J. Zhai, and Q. Y. Chen. Evaluation of Various Turbulence Models in Predicting Airflow and Turbulence in Enclosed Environments by CFD : Part 2 — Comparison with Experimental Data from Literature Evaluation of Various Turbulence Models in Predicting Airflow and Turbulence in Enclo. *HVAC&R Research*, vol. 9669, n. February 2016, pp. 37–41, 2011.

[10] K. Shimada and T. Ishihara. Kinematics and Dynamics of Sphere. vol. 16, pp. 575–585, 2001.